

Report of Test

Absolute Spectral Radiance Responsivity

of the

NASA GLAMR exIGA Radiometer L-1 model 8350, S/N 002

Request Submitted by:

Joel McCorkle
NASA Goddard Space Flight Center
Greenbelt, MD

1. Description of Calibration Items

The device under test (DUT) is an extended-InGaAs radiance meter manufactured by L-1 Standards and Technology, Inc. (L-1), model 8350, S/N 002. The device is housed in a 2-inch diameter tube with a fore-optic consisting of an aperture and lens. The detector is temperature controlled (L-1 model 3100-1L, S/N 12132) and the rear of the device has inputs for the L-1 temperature controller and a BNC output for the detector signal. The detector came with an L-1 model 3300v2, S/N 008, transimpedance amplifier which was used for the calibration. Figure 1.1 shows the detector and accessory equipment as received.



Figure 1.1 Picture of GLAMR exIGA Radiometer.

1.1 Calibration Request

The request was to calibrate the DUT for absolute radiance responsivity from 1600 nm to 2500 nm with a standard uncertainty of 3.0 % (k=1) or better for the range 1600 nm to 2300 nm and 10 % (k=1) or better for the range 2300 nm to 2500 nm.

2. Description of Test

The detector was characterized for absolute spectral radiance responsivity on the NIST facility for Spectral Irradiance and Radiance responsivity Calibrations using Uniform Sources (SIRCUS).^{1,2} The calibration took place in various stages from May 1, 2019 to Aug. 7, 2019. During each calibration test, the detector was temperature controlled at -20.0 °C by the L-1 controller and checked at the beginning and end of each calibration session.

This calibration was performed in a slightly different way compared to the conventional SIRCUS technique in that a pyroelectric detector (GenTec Model SDX-1005, S/N: 507097 with power supply Model: STEP, S/N: 507099) was used as the working reference detector and therefore required that the measurements were collected in AC mode using an optical chopper. The pyroelectric detector used was loaned to NIST from NASA and labeled as “NASA pyro #2 5 mm.” Measurements were also simultaneously made using a near-equivalent NIST-purchased pyroelectric detector (GenTec Model SDX-1237, S/N: 507568 with power supply Model: STEP, S/N: 507569), but the analyses reported here were completed with the NASA pyro due to having higher responsivity.

Overall, the calibration was performed in three parts. First, an irradiance responsivity scale transfer was performed from a SIRCUS trap detector, T-01, at a few tie points from 690 nm to 915 nm, to the NASA pyroelectric detector. Second, a reflectance measurement was made for a witness sample representative of the pyroelectric detector (using an infrared spectrometer in diffuse reflectance mode with an integrating sphere). Assuming the responsivity curve of the pyroelectric detector is proportional to its absorptance (computed as 1 minus reflectance), the first two parts were used to determine the spectral irradiance responsivity of the pyroelectric sensor. Third, an absolute radiance responsivity measurement was made from 1600 nm to 2500 nm of the DUT against the calibrated pyroelectric detector using chopped, AC mode detection.

Description of laser systems used: Several laser systems were used to cover the specified ranges for the various parts of the calibration.

1. Ti:Sapphire laser (Continuous Wave, CW) was used for the scale transfer step between T-01 and the pyroelectric detector. Measurements were taken using both the “DCM” output coupler (689 nm to 757 nm) and the Mid-Wave output coupler (800 nm to 900 nm).
2. Three lasers were used for the absolute radiance responsivity calibration of the DUT:
 - a. Picosecond mode-locked LBO-OPO laser from 1567 nm to 1765 nm using the idler output from the main cavity.
 - b. Argos SF-15 Module B (CW) from 1660 nm to 1880 nm using the signal output.
 - c. IPG Cu²⁺:ZnS/Se laser (CW) from 1896 nm to 2519 nm.

The output from the lasers was coupled to an optical fiber. The Ti:Sapphire and LBO-OPO lasers

used Low-OH silica fiber while the Argos SF-15 and IPG Cu²⁺: ZnS/Se used 200 μm core ZrF₄ fiber. The optical fiber was in turn connected to a side port on the SIRCUS integrating sphere and illuminated an area toward the front of the sphere. For the Ti:sapphire laser, a section of fiber was placed into an ultrasonic bath to reduce effects due to laser speckle. For the LBO-OPO system, the ultrasonic bath was not required and for the Argos SF-15 and IPG Cu²⁺: ZnS/Se lasers no speckle reduction was used. For the Ti:sapphire laser, a BEOC laser power controller stabilized the beam to less than the 0.1 % level using feedback from a photodiode in the sphere, removing short term as well as long term fluctuations in the power output from the laser source. For the lasers used in the absolute radiance responsivity calibration, a power controller was not used due to poor performance in the longer wavelength ranges and/or due to low signals on the pyroelectric detector, where the use of a power controller further reduces the pyroelectric detector signal due to reduced laser power throughput to the source sphere.

A Coherent WaveMaster (S/N: W0385) measured the air wavelength for the Ti:Sapphire laser, a Bristol 621 wavemeter (S/N: 6208) measured the vacuum wavelength for the LBO-OPO system, and a Burleigh wavemeter (S/N: 0024213) measured the air wavelength for the Argos SF-15 and IPG Cu²⁺: ZnS/Se lasers. All wavelengths were converted to the air value for data analysis. In the case of the LBO-OPO idler, the signal wavelength was measured directly, and the actual wavelength value was determined as,

$$\lambda_{idler} = \frac{1}{\left(\frac{1}{\lambda_{pump}} - \frac{1}{\lambda_{signal}}\right)} 1.00027 \quad (2.1)$$

where λ_{pump} is 532.2 nm, λ_{signal} is measured by the Bristol wavemeter, and 1.00027 converts the vacuum measurement to air.

Integrating Sphere: The integrating sphere used for radiance responsivity was a LabSphere 30.48 cm (12”) diameter, Spectralon-coated sphere equipped with a 5.08 cm (2”) diameter exit aperture fabricated by LabSphere (non-point source geometry). For the irradiance scale transfer measurements, a 2-inch Thorlabs sphere (IS200-4, SN M00251969) with ~ 1.27 cm (0.5”) diameter aperture port was used due to limitations incurred from the small working distance.

Data Acquisition and Control Program: The spectral data was acquired using a modified version of the SIRCUS Labview program. Here, the time-dependent waveforms of the chopped signals are collected by an NI USB-6211 data acquisition module (S/N: 1A98ECC) sequentially for each of the detectors (DUT or working standard) along with the simultaneously recorded monitor signal into separate analog input channels (differential mode). The data is analyzed after each square waveform collection to give the DC signal as the difference between the average peak and valley signals for each cycle in the waveform for both the detector and the monitor. This results in an array of DC signals for both the detector and monitor, which are then ratioed. The chopping frequency was 10 Hz while the data acquisition was completed at 10 kHz sampling rate. It should be noted that the analysis method results in rejection of 1 cycle in the waveform.

Statistics were determined in two different ways. In one way, a long waveform was collected, where, for example, a 1-minute waveform was collected with 10 chopper cycles per second yielding 599 samples of the DC signal. The average and standard deviation of the mean for these samples was reported. In the other way, short waveforms were collected, where, for example, 0.5

second waveforms were collected, and the 4 resulting samples were averaged. The 0.5 second collections were then repeated multiple times. The average and standard deviation of the mean were then determined for the repeated 0.5 second collections. In some cases, the two methods just described were also subsequently repeated and the average and percent standard deviation of those repeats was determined. The second way was more convenient for rejecting pulses where significant deviation in the signal level during the timescale of a single 100 ms pulse precludes the analysis method. For the CW lasers, either analysis method works as the waveforms were quite stable and the occurrence of “bad” pulses was rare. The former method was used for the Ti:Sapphire and IPG Cu²⁺/ZnS:Se lasers. For the LBO-OPO laser, the occurrence of “bad” pulses was more prevalent, and the latter method is needed. In general, the latter method could be preferred due to easier pulse rejection and was used with the Argos SF-15 laser.

Two versions of the Labview program were used:

1. The version where long waveforms are collected is: Chopping SIRCUS_V2.vi
2. The version where short waveforms are repeated is: Chopping SIRCUS_V3.vi

Both versions are stored on the SIRCUS computer and backed up on the internal network at:

C:\Labview Programs\SIRCUS chopping
\\cfs2e.nist.gov\685\internal\G04\Sircus\SIRCUS\Software_LabView\SIRCUS chopping

Description of calibration detectors: The working standard trap detector T-01 was used to determine the irradiance responsivity of the NASA pyroelectric detector at several tie points. It was equipped with an aperture having an area of 19.6591 mm². A precision transimpedance amplifier, Prec#2, was used with the trap detector. The trap gain was set to 1 x 10⁴ V/A for all measurements. T-01 was previously calibrated for irradiance responsivity with scales traceable to the NIST Primary Optical Watt Radiometer (POWER).³ The responsivity scale for T-01 is derived from a SIRCUS calibration using T-06 as the reference standard detector,⁴ where T-06 was calibrated directly against POWER.^{5,6}

For the absolute radiance responsivity calibration, the working standard detector was the NASA pyro #2 5 mm with a scale traceable to NIST POWER as explained in the preceding paragraph. It was equipped with an aperture having an area of 9.6 mm² (National Aperture model 1-3500+B-2+M-1, uncalibrated). The pyroelectric detectors have an internal current-to-voltage converter and operate at a fixed gain, so the signals were measured in units of volts.

The monitor detector was an L-1 Standards and Technology, Model VNS-1 and S/N 102, integrating sphere photodiode with Si, IGA, and exIGA detectors. The exIGA detector was used for the radiance responsivity calibration and temperature stabilized at -22.0 °C using the L-1 Model 3100 Temperature controller. An L-1 Model 3300v2 transimpedance amplifier (S/N: 3300v2-011) was also used. In this case the monitor detector was moved to each laser table and measured an ~ 4 % pickoff of the laser beam from a CaF₂ window. The output from the transimpedance amplifier was collected by the DAQ module into analog input channel 0. For the irradiance responsivity scale transfer, a silicon photodiode mounted to the integrating sphere was used for the monitor signal.

3-axis stage: The integrating sphere is mounted on an XYZ translation stage, with the Z-position (along the optical axis) measured with a linear encoder. The X- and Y-axes enable the source to

be properly positioned in front of an instrument before it measures the sphere radiance. The Z-position is used to accurately determine the separation between relevant apertures.

Measurement Setup: Detectors used in these experiments were mounted to tip-tilt stages and aligned to the optical axis of the integrating sphere source using a double-headed laser. Here, two different integrating spheres were used to accomplish different parts of the calibration. A 2" diameter Thorlabs sphere (small) with 1.27 cm diameter (0.5") aperture and the 12" diameter LabSphere sphere (large) with 5.08 cm (2") diameter aperture were used. To align the detectors to the large sphere, the double-headed laser was first mounted in-front of the large sphere where one end of the laser was previously aligned to the center of the sphere aperture. The other end of the laser was retroreflected from a glass microscope slide on each detector to align to the optical axis. Lastly, the laser was centered on each detector using the 3-axis stage to determine the X,Y position. For the small sphere, the double-headed laser was mounted to the rails of the z-axis stage and the X,Y position for each sphere relative to that laser position was found. Knowing the difference in position between the two spheres and the position of the large sphere for each detector allowed the position of the small sphere for each detector to be determined. See Figures 2.1 and 2.2 for photographs of the measurement setup.

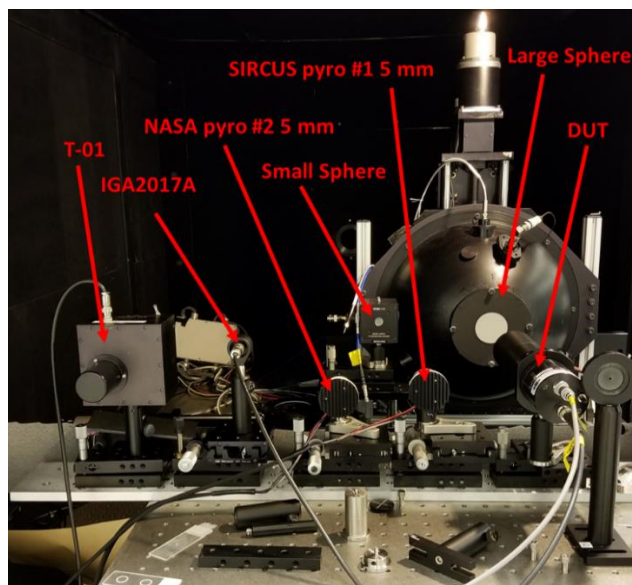


Figure 2.1 Back-view of detector bench setup.

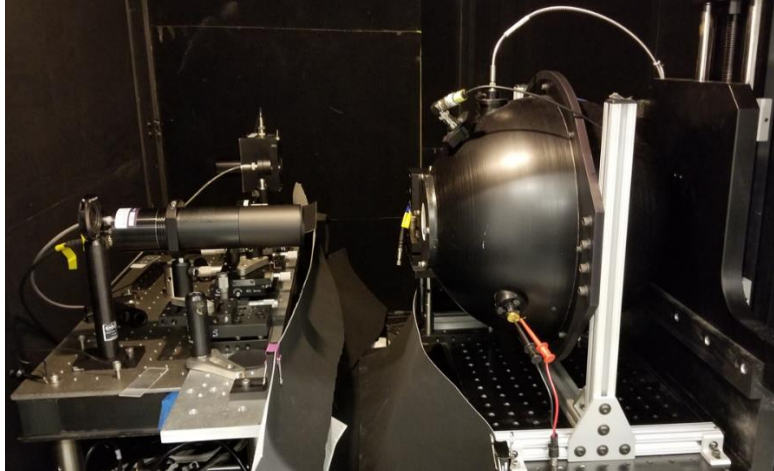


Figure 2.2 Side-view of detector bench setup for radiance measurements of the DUT.

2.1 Irradiance Responsivity scale transfer from T-01 to NASA pyro #2 at tie points

An irradiance measurement was performed to transfer the irradiance responsivity scale from T-01 to NASA pyro #2 at some tie points (688.6 nm, 715.5 nm, 757.3 nm, 802.9 nm, 849.4 nm and 902.1 nm). The integrating sphere source (ISS) was the small sphere and was equipped with a 1.27 cm (0.5”) diameter aperture. All measurements for this part were done with the sphere at $z = -570.255$ mm. The detector positions were determined radiometrically as described in Section 3.2, below, and yield the working distance along with the known Z-position.

Due to the small responsivity of the pyroelectric detector, the sphere needed to be placed at a Z-position close enough to obtain reasonable signal-to-noise. Using the typical 12” LabSphere at such a close Z-position produces errors for T-01, where the light entering the aperture overfills the tunnel trap detectors. By using the small sphere, we were able to complete the scale transfer at the same Z-position for both detectors, while maintaining good signal-to-noise for the pyroelectric detector.

2.2 Reflectance of pyro witness sample

To generate a complete irradiance responsivity scale for the pyroelectric detector traceable to NIST POWR from T-01 as described in Section 2.1, the reflectance of the pyroelectric detector must be known. We assume that the responsivity of the pyroelectric detector is proportional to its absorptance, which is given by $1 - R$ when $T \sim 0$, where R is the Reflectance and T is the transmittance. Therefore, the reflectance curve can be scaled to the irradiance responsivity using the tie points determined in Section 2.1 and the complete irradiance responsivity scale of the pyroelectric detector is realized.

The absorptance of the pyroelectric detector is determined by the optical properties of the coating which absorbs light and transfers heat to the pyroelectric crystal. Due to limitations imposed by the detector housing and the minimum beam diameter of the reflectance-measurement facility, it has not yet been possible to measure the directional hemispherical reflectance of the actual pyroelectric detector. Instead, the directional hemispherical reflectance of a larger witness detector

was used. The witness detector consisted of a 9 mm diameter pyroelectric “detector” manufactured as a witness specifically by Gentec in an identical manner as the actual 5 mm detector. It has the same black coating on the same pyroelectric element with the same gold coating on the back of the detector element, but is mounted in its housing in a way that provides complete hemispherical access to the front surface, enabling it to be placed optimally against an integrating sphere for complete collection of the diffuse reflected light. It has no electrical connections and so is not a real detector, but is otherwise optically identical to a real detector. The directional-hemispherical reflectance of the 9 mm diameter witness detector was measured by Leonard Hanssen at the NIST Fourier Transform Infrared Spectrophotometry (FTIS) facility using a diffuse gold integrating sphere from 834 nm to 3393 nm.⁷ The witness detector reflectance was also found to be nearly Lambertian with zero specular component within its expanded uncertainty.

2.3 Radiance Responsivity

Absolute radiance responsivity measurements for the DUT (with associated transimpedance amplifier) versus the NASA pyroelectric detector #2 were completed at discrete wavelengths between 1600 nm to 2500 nm using the SIRCUS facility in the chopped, AC mode configuration. The ISS was the 12” diameter sphere described in Section 2 with a 5.08 cm (2”) aperture. The sphere was placed at a Z-position of ~ -587 mm. This Z-position was approximately 20 cm away from the front aperture of the DUT, which placed the field of view completely within the 2-inch diameter sphere output aperture and was also appropriate to obtain good signal-to-noise for the pyroelectric working reference detector. An X-Y response map for the DUT was also measured, verifying the central position and underfilled configuration of the DUT relative to the sphere aperture. The working distance for the pyroelectric working reference detector was determined from the sphere Z-position and the radiometrically determined detector position, described in Section 3.2 below.

3. Results of Test

For this calibration, both an irradiance and a radiance measurement were performed. In both cases, the reference detector (trap T-01 for the scale transfer step and NASA pyro #2 for the absolute radiance responsivity measurement of the DUT) establishes the irradiance or radiance emitted from the source sphere. Even though NASA pyro #2 is an irradiance meter, it is used to determine the radiance of the source, requiring knowledge of the solid angle of the source. To determine the solid angle, the distance between the trap aperture and the integrating sphere source aperture was measured, along with the integrating sphere and trap aperture areas, see Section 3.1. For the irradiance measurements performed in the scale transfer step, the irradiance of the source must be known at the test detector (NASA pyro #2 5 mm) reference plane. This is done by applying a correction factor to the measured source irradiance at the reference detector reference plane that is derived from the relative positions of the two detectors. The detector positions are determined radiometrically, as described in Section 3.2, and the distance of each from the source is determined by measuring the Z-position with the linear encoder on the Z-axis stage.

3.1 Determination of the sphere source radiance

The radiance of the sphere source was determined with the flux transfer method. A working reference detector (NASA pyro #2 5 mm) measured the radiant power from the sphere source passing through two precision apertures, one on the source side, another on the detector side.

The radiance L [$\text{W m}^{-2} \text{sr}^{-1}$] of the sphere is determined from radiant power P [W] and the geometric extent G by:

$$L = \frac{P}{G} \quad (3.1)$$

The geometric extent G [$\text{m}^2 \text{sr}$] is given by

$$G = \frac{\pi^2}{2} [(d^2 + r_s^2 + r_D^2) - \{(d^2 + r_s^2 + r_D^2)^2 - 4r_s^2 r_D^2\}^{1/2}] \quad (3.2)$$

where r_s is the radius of the aperture in front of the source, r_D is the radius of the aperture in front of the detector, and d is the distance between the two apertures. The diameter of the sphere aperture was large enough (50.8 mm) to overfill the radiance measurement angle of the DUT radiometer by the sphere output radiation. The distance, d , was chosen large enough (238.81 mm) so that the sphere aperture was well within the acceptance angle of the working reference detector for power measurement.

3.2 Detector offset and offset uncertainty determination for irradiance meters

For both radiance and irradiance measurements, knowledge of a distance between the source and a detector aperture is required. For the irradiance measurements in the scale transfer step, the distance for both T-01 (the working reference) and NASA pyro #2 (the test detector) was determined relative to the *small* sphere. For the radiance measurement, only the distance for the working reference detector (now NASA pyro #2) was determined relative to the *large* sphere. All distances were determined radiometrically.

In general, at several different Z positions, the detector and monitor voltages were recorded to yield a relative irradiance. Using the $1/Z^2$ law for on-axis irradiance (inverse square law) the resultant data can be fit to a point-source geometry (Equation 3.3) and a non-point-source geometry (the experimental configuration, Equation 3.4) to yield the Z-position of the detector aperture plane. From the Z-position encoder reading used in the radiance and irradiance measurements and the detector Z-position from the radiometric $1/Z^2$ law fit, the actual detector aperture to sphere aperture distance in millimeters was determined. Figure 3.1 is a schematic of the configuration.

The inverse square law fitting equation for a point-source geometry is:

$$y = \frac{m_1}{(M_0 - m_2)^2} \quad (3.3)$$

Where y is the relative irradiance, m_1 is a fitting constant, M_0 is Z-position of the integrating sphere that is read by the Z-encoder, and m_2 is the Z-position of zero offset between the two apertures. The uncertainty in m_2 , for the sphere position during calibration, gives the uncertainty in the distance between the two apertures.

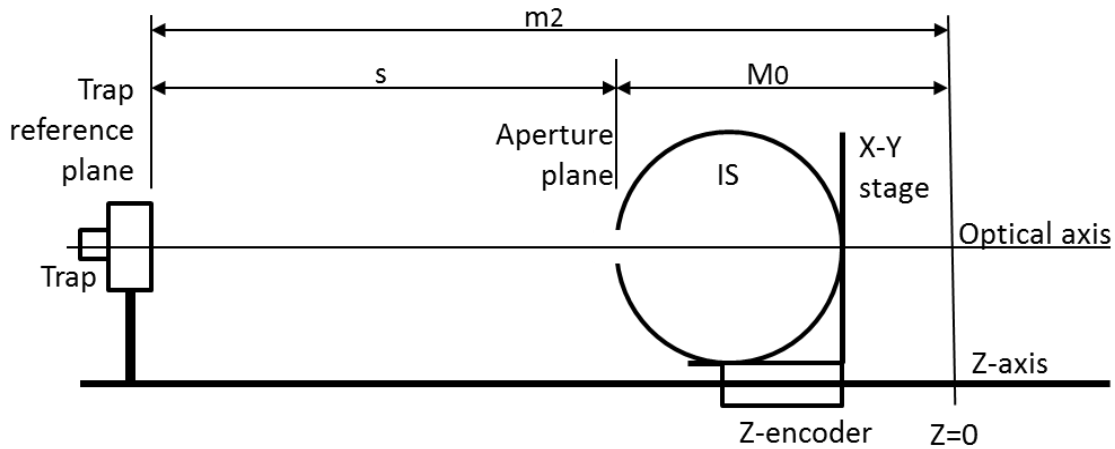


Figure 3.1. Schematic of the configuration for determining trap-sphere distance radiometrically.

If the source aperture is large, the data can be fit to a non-point source geometry by fitting the data to the expression:

$$y = \frac{m_1}{((M_0 - m_2)^2 + m_3^2 + m_4^2)} \quad (3.4)$$

where y , m_1 , M_0 , and m_2 are the same as in Eq. 3. $m_3 = r_d$, the radius of the detector aperture, and $m_4 = r_s$, the radius of the integrating sphere aperture. Equation 3.4 is valid in the limit where

$$(r_s^2 + r_d^2 + s^2) \gg 2r_s r_d \quad (3.5)$$

The inverse square law measurements along with the fit to equation 3.4 for each detector can be seen in Figures 3.2 through 3.4, below. At the minimum separation, s , used for each distance measurement, the ratio given by equation 3.5 was determined for each detector. This result is summarized in Table 3.1 and shows the condition of equation 3.5 holds and that equation 3.4 is valid in each case. Even though the ratio from equation 3.5 is somewhat small, no improvement in the fit was observed from removing points at small separation distances. Furthermore, the residuals are approximately 3 orders of magnitude smaller than the base measurement and show there is no obvious bias or offset. The fitting results are also summarized in Table 3.2.

Table 3.1 Results of Eq. 3.5 at minimum separation distances.

Detector	Sphere	Test	r_s (cm)	r_d (cm)	s (cm)	Ratio (Eq 3.5)
NASA pyro #2	Large	Radiance	2.54	0.175	12.5	183
NASA pyro #2	Small	Irradiance	0.635	0.175	12.4	693
T-01	Small	Irradiance	0.635	0.25	20	1260.6

Table 3.2 Results of the inverse square law fits of equation 3.4 to the data.

Detector	Sphere	Test	m_2 (mm)	Fitting Uncertainty (mm) (k=1)	R, fit
NASA pyro #2	Large	Radiance	-825.15	0.27102	0.99999
NASA pyro #2	Small	Irradiance	-824.09	0.31948	0.99999
T-01	Small	Irradiance	-817.23	0.00744	1

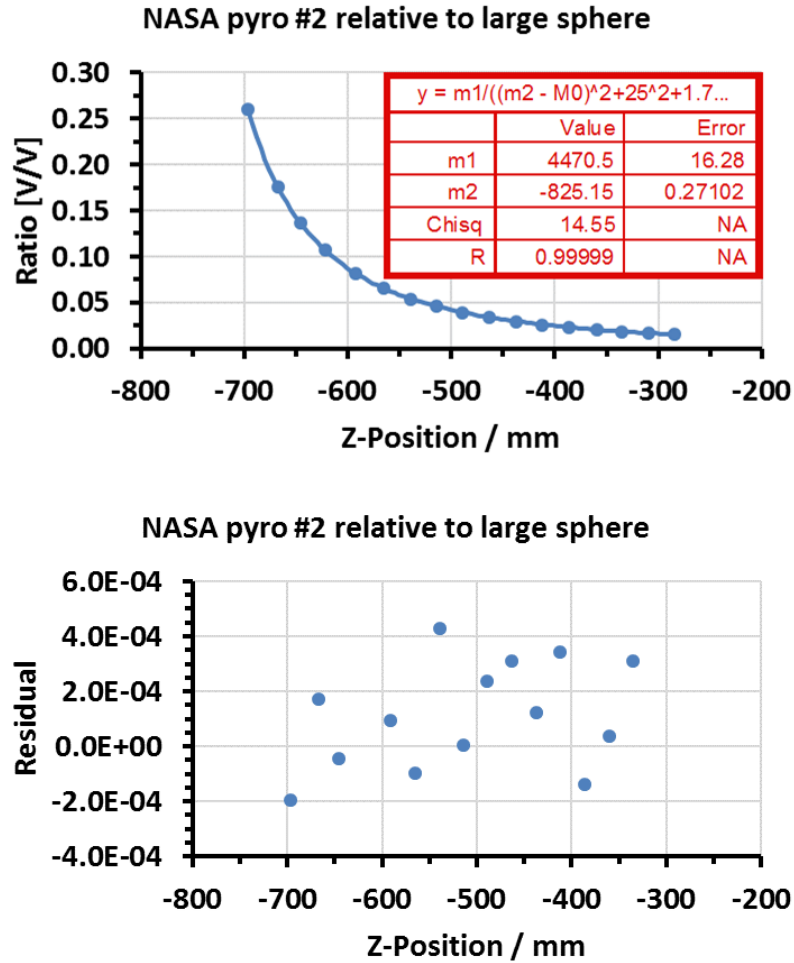


Figure 3.2 Offset and uncertainty fit to a non-point source geometry at a wavelength of 850 nm (top) and Residuals from the fit of Eq. 3.4 to the irradiance response data (bottom) relative to the large sphere for distance determination of the working standard reference detector, NASA pyro #2, in the radiance measurement of the DUT.

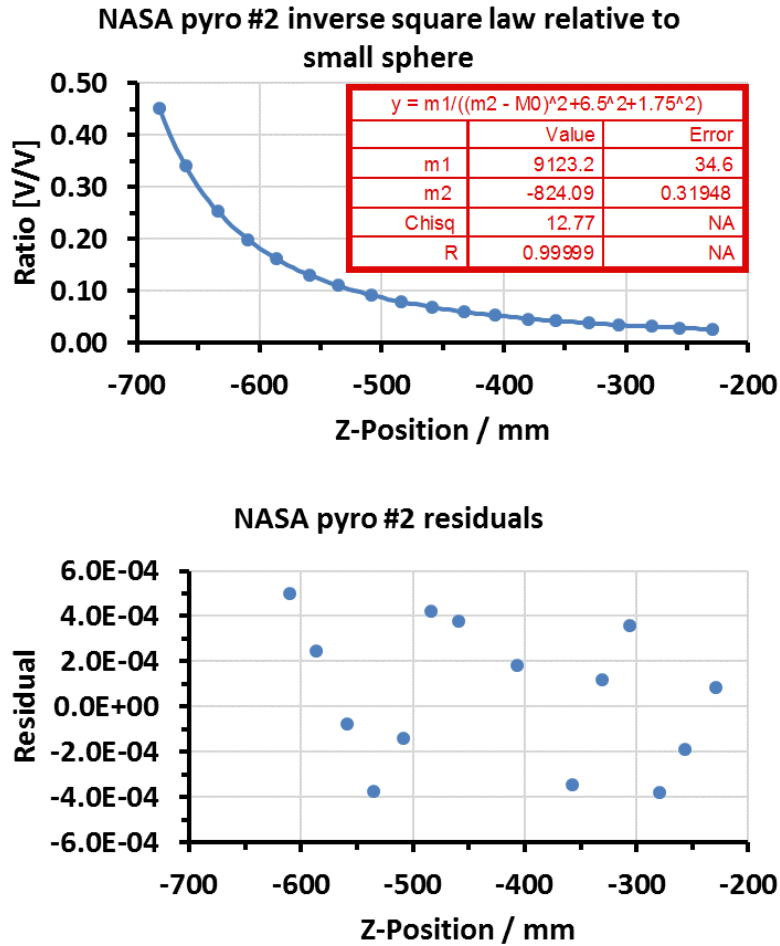


Figure 3.3 Offset and uncertainty fit to a non-point source geometry at a wavelength of 715 nm (top) and Residuals from the fit of Eq. 3.4 to the irradiance response data (bottom) relative to the small sphere for distance determination of NASA pyro #2, in the irradiance scale transfer measurement.

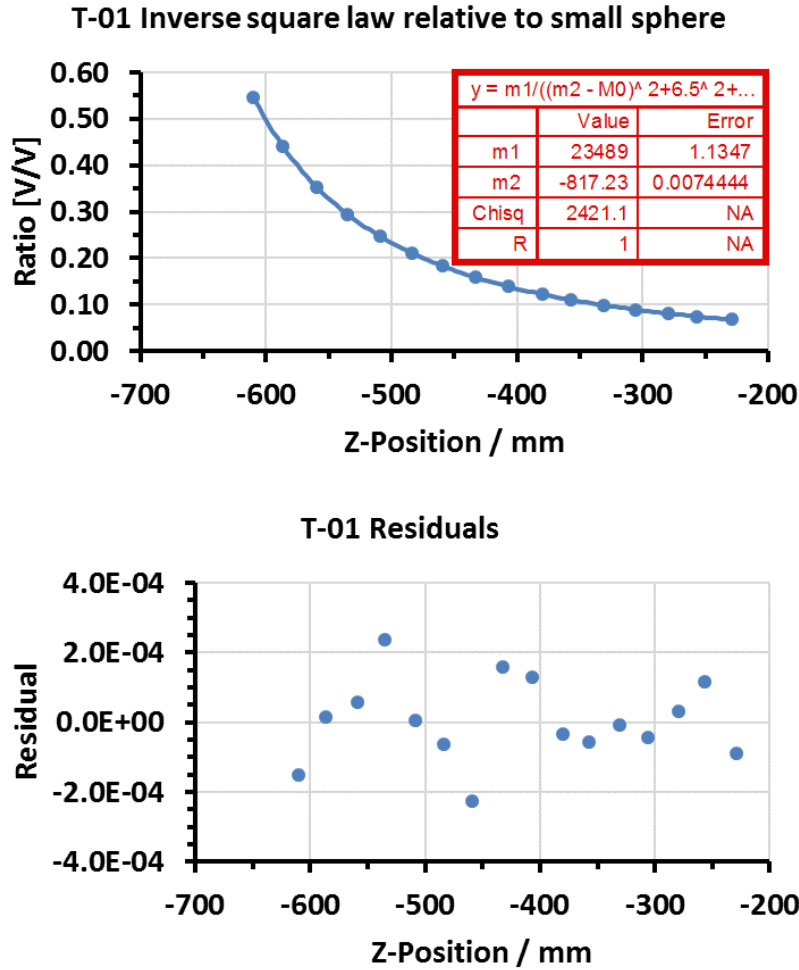


Figure 3.4 Offset and uncertainty fit to a non-point source geometry at a wavelength of 715 nm (top) and Residuals from the fit of Eq. 3.4 to the irradiance response data (bottom) relative to the small sphere for distance determination of T-01 in the irradiance scale transfer measurement.

3.3 Irradiance responsivity scale transfer from T-01 to NASA pyro #2

The irradiance responsivity of NASA pyro #2 was determined against T-01 using the Thorlabs 2” integrating sphere with 0.5” aperture as the source. Waveforms were collected for 40 seconds yielding 399 samples of the detector signal. At each wavelength, the irradiance responsivity was repeated at least 3 times. The average and standard deviation of the repeat measurements were determined and are displayed in Figure 3.5 and Table 3.3.

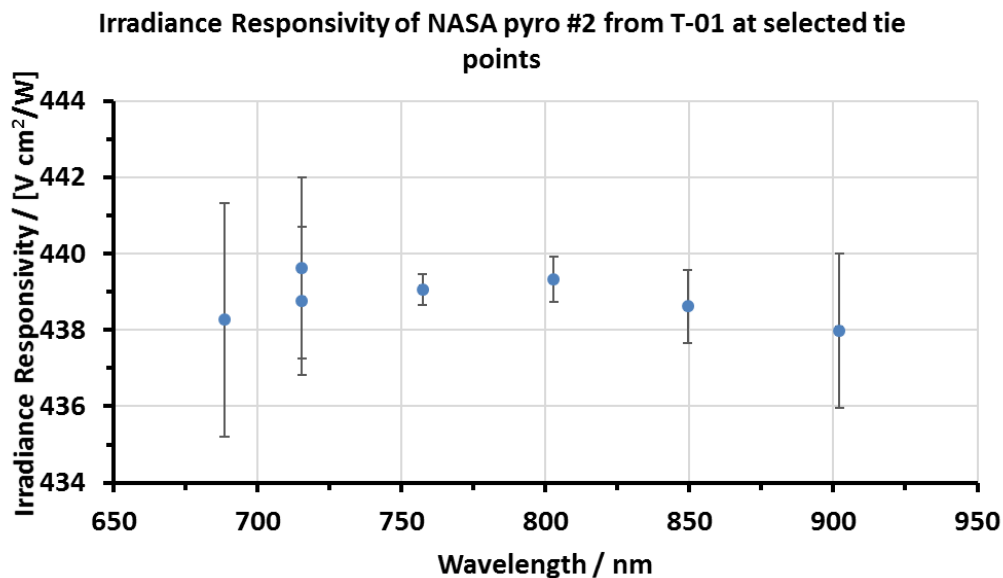


Figure 3.5 Irradiance Responsivity for NASA pyro #2 from T-01 at selected tie points between 690 nm to 900 nm.

Table 3.3 Irradiance Responsivity Data for NASA pyro #2 at selected tie points.

Wavelength [nm]	Irradiance Responsivity [V cm ² / W]	% St.Dev.
688.622	4.383E+02	6.978E-01
757.322	4.391E+02	9.021E-02
715.471	4.396E+02	5.396E-01
802.882	4.393E+02	1.346E-01
902.074	4.380E+02	4.614E-01
849.404	4.386E+02	2.195E-01

3.4 Reflectance of witness sample and pyroelectric detector irradiance responsivity scale

The directional-hemispherical reflectance of the pyro witness detector was measured from 834 nm to 3394 nm as shown in Figure 3.6. As explained above, the absorptance of the witness sample is given by $1-R$, which is assumed to be proportional to the pyro responsivity spectrum. Knowing the irradiance responsivity at a tie point (or set of tie points), the absorptance spectrum was shifted according to equation 3.6 to yield the irradiance responsivity scale, where the absorptance is given by $1-R$ and I is the irradiance responsivity. In this case, the tie point was chosen at 849.4 nm, where the irradiance responsivity and reflectance measurements both overlap and have the smallest measurement error. The resulting irradiance responsivity spectrum for NASA pyro #2 is shown in Figure 3.7.

$$I_{pyro}(\lambda) = \left[\frac{(1 - R(\lambda))}{1 - R(\lambda = \text{tie point})} \right] I(\lambda = \text{tie point}) \quad (3.6)$$

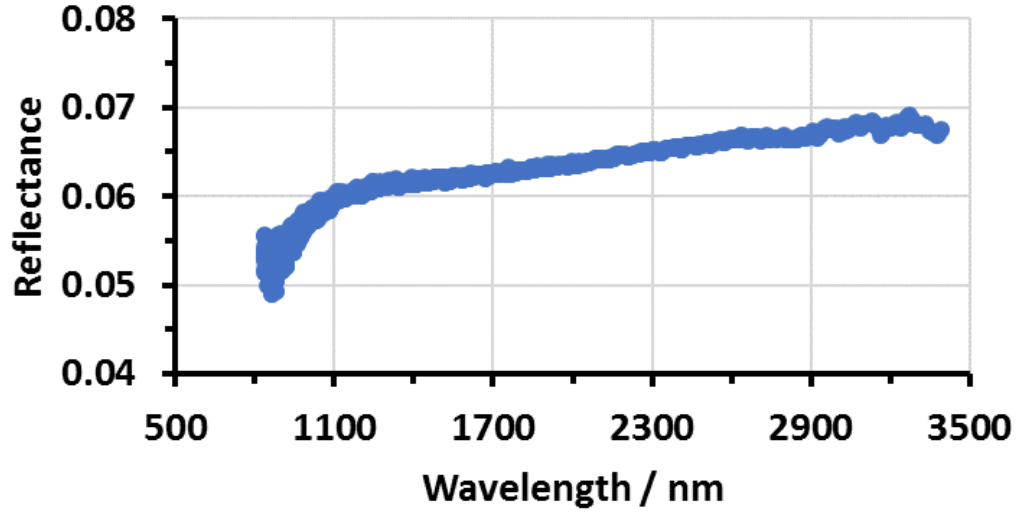


Figure 3.6 Directional-hemispherical reflectance of the pyro witness detector.

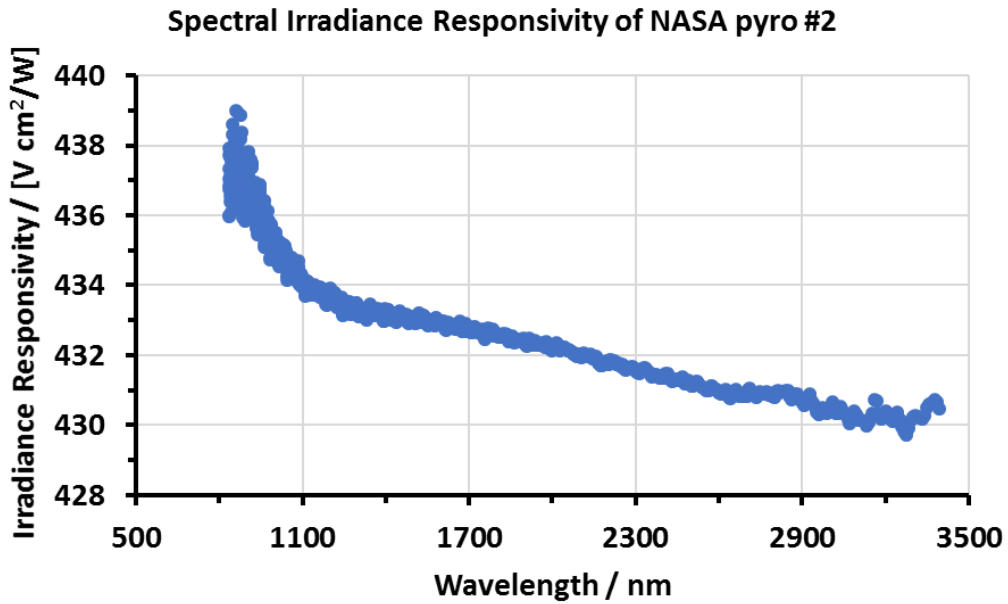


Figure 3.7 Irradiance responsivity of NASA pyro #2 from 834 nm to 3394 nm from T-01.

3.5 Uncertainty analysis for the irradiance responsivity scale of NASA pyro #2

Table 3.4 Uncertainty Budget for Absolute Spectral Irradiance Responsivity of NASA pyro #2.

	Relative Standard Uncertainty [%]
Uncertainty Component	Tie point at 849.4 nm and reflectance from 834 nm to 3394 nm
Reference detector Irrad. Cal. (T-01 from T-06)	0.09
Irradiance Measurement Standard Deviation at tie point (849.4 nm)	0.22
Amplifier gain	N.A.
Geometry Alignment	0.05
Reference Detector Aperture Area	0.02
Distance	0.13
Reference Detector Uniformity	N.A.
Wavelength	0.01
Witness sample absorptance % St Dev ¹	0.22
Combined Standard Uncertainty (k=1)	0.35

Note 1: This entry is the average % St. Dev. over the full spectral range. Higher standard deviations around 0.3 % to 0.5 % are noted for the range below 900 nm.

Note 2: This is not the full calibration uncertainty budget. The uncertainty budget, Table 3.4, does not include environmental effects on both the reference detector and the GLAMR radiometer. The uncertainty budget in Table 3.4 does not include measurement uncertainties associated with the pyroelectric detector itself. No evaluations of instrument performance characteristics such as temperature dependence, response linearity or temporal stability were performed. For estimates in the interpolated uncertainty, see the reference.⁸

3.6 Radiance responsivity of GLAMR exIGA

With knowledge of the absolute spectral irradiance responsivity of the pyroelectric detector, NASA pyro #2, it was used as the working reference standard detector in the radiance responsivity calibration of the DUT, the GLAMR exIGA radiometer. Measurements were done at a fixed Z-position of ~ -587 mm using the large sphere as the source. This Z-position ensured the field-of-view of the DUT was entirely filled by the integrating sphere exit aperture and was close enough for good signal-to-noise with the pyroelectric detector. This Z-position also corresponded to a working distance of 23.8 cm for the reference standard detector. The gain setting on the

transimpedance amplifier for the DUT was 1×10^5 V/A for all measurements.

Because the pyroelectric detector was used, the radiance measurements were also collected in AC mode with an optical chopper in the laser source path. Waveforms were collected at a sampling rate of 10 kHz with a 10 Hz chopping frequency. For the IPG $\text{Cu}^{2+}:\text{ZnS}/\text{Se}$ laser, 40 second waveforms were collected, corresponding to 399 measurements of the DC signal. For the LBO-OPO and Argos SF-15 (module B) lasers, 0.5 second waveforms were collected and repeated 120 times (1 minute of data). The one-minute collection was also repeated several times to yield an average and percent standard deviation for the radiance responsivity. The resulting radiance responsivity of the DUT, GLAMR exIGA, is shown in Figure 3.8.

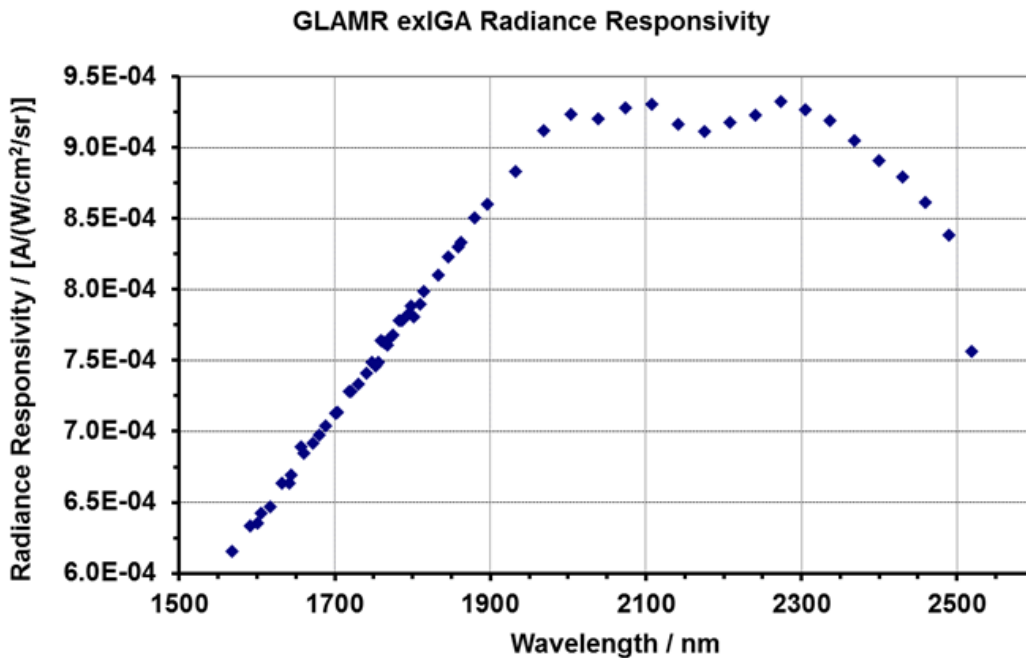


Figure 3.8 Radiance responsivity of GLAMR exIGA radiometer from NASA pyro #2.

Table 3.5 Tabulated absolute spectral radiance responsivity data for GLAMR exIGA.

Wavelength [nm]	Radiance Responsivity [A/(W/cm²/sr)]	% Uncertainty (k=1)
1567.2	6.155E-04	1.22
1591.3	6.331E-04	1.16
1600.4	6.351E-04	0.45
1605.0	6.421E-04	0.68
1617.3	6.471E-04	0.42
1632.4	6.632E-04	0.80
1641.8	6.635E-04	0.38

REPORT OF TEST

Absolute Spectral Radiance Responsivity of NASA GLAMR exIGA Radiometer

1643.8	6.690E-04	0.43
1657.0	6.893E-04	0.41
1659.8	6.847E-04	0.44
1671.6	6.914E-04	0.37
1680.2	6.971E-04	0.40
1688.2	7.037E-04	0.63
1701.2	7.125E-04	0.43
1703.0	7.132E-04	0.41
1719.0	7.279E-04	0.41
1721.1	7.285E-04	0.38
1729.9	7.332E-04	0.40
1740.8	7.408E-04	0.43
1748.3	7.488E-04	0.45
1752.1	7.459E-04	0.37
1755.8	7.488E-04	0.45
1759.5	7.639E-04	0.39
1763.4	7.627E-04	0.38
1767.1	7.611E-04	0.41
1771.0	7.659E-04	0.40
1774.9	7.679E-04	0.39
1782.6	7.782E-04	0.37
1786.4	7.784E-04	0.40
1794.3	7.823E-04	0.37
1798.2	7.886E-04	0.41
1802.1	7.805E-04	0.42
1809.8	7.896E-04	0.44
1814.0	7.986E-04	0.45
1833.4	8.103E-04	0.44
1845.6	8.227E-04	0.47
1858.4	8.300E-04	0.37
1862.5	8.335E-04	0.46
1879.7	8.503E-04	0.54
1896.3	8.599E-04	0.48
1932.5	8.834E-04	0.39
1968.4	9.122E-04	0.39
2003.7	9.236E-04	0.38
2038.8	9.203E-04	0.38
2073.6	9.283E-04	0.38
2107.9	9.310E-04	0.43
2141.9	9.167E-04	0.44
2175.5	9.116E-04	0.43
2208.5	9.179E-04	0.43
2241.3	9.229E-04	0.44

2273.6	9.326E-04	0.44
2305.6	9.268E-04	0.45
2337.1	9.193E-04	0.49
2368.5	9.050E-04	0.48
2399.5	8.912E-04	0.46
2429.9	8.791E-04	0.47
2459.9	8.615E-04	0.50
2489.5	8.384E-04	0.43
2518.9	7.563E-04	0.55

3.7 Uncertainty analysis for the Radiance Responsivity of GLAMR exIGA

Table 3.6 Uncertainty budget for absolute spectral radiance responsivity of GLAMR exIGA.

Uncertainty Component	Relative Standard Uncertainty [%]		
	1567 nm to 1721 nm (LBO-OPO)	1659 nm to 1880 nm (Argos SF-15 Module B)	1896 nm to 2519 nm (IPG Cu ²⁺ :ZnS/Se)
Reference detector Irrad. Cal. (NASA pyro #2 from T-01)	0.34	0.34	0.34
Measurement % St Dev of the Mean	0.42	0.19	0.24
Distance	0.12	0.12	0.12
Geometry Alignment	0.05	0.05	0.05
Amplifier Gain	N.A.	N.A.	N.A.
Reference Detector Uniformity	N.A.	N.A.	N.A.
Sphere Aperture Area	0.05	0.05	0.05
Wavelength	0.01	0.01	0.01
Total % Uncertainty (k=1)	0.60	0.42	0.44

Note 1: This is not the full calibration uncertainty budget. The uncertainty budget, Table 3.4, does not include environmental effects on both the reference detector and the GLAMR radiometer. The uncertainty budget in Table 3.4 does not include measurement uncertainties associated with the pyroelectric detector itself. No evaluations of instrument performance characteristics such as temperature dependence, response linearity or temporal stability were performed. For estimates in the interpolated uncertainty, see the reference.⁸

4. General Information

It should be noted that the reported results were derived from using the dial gain value on the provided amplifiers (i.e. 1×10^5 V/A) to give the radiance responsivity in $[A/(W/cm^2/sr)]$. This assumes that the transimpedance amplifier for each DUT has been calibrated and the dial gain values have high accuracy (to say 0.05 % or better). If this is not the case, we need either to obtain the gain correction factors for those amplifiers or can only report the calibration for each device as a whole system (i.e. detector plus amplifier) in units of $[V/(W/cm^2/sr)]$ for radiance.

The calibration measurements were performed by Brian G. Alberding and John T. Woodward using the VisSIRCUS laboratory and the Chopping SIRCUS_V2 and _V3 data acquisition programs.

Information was recorded in the SIRCUS Vis #20 laboratory notebook, pp.75-103.

The data were reduced by Brian Alberding.

This calibration required 11 days of laboratory work (including setup, troubleshooting, and data collection) on SIRCUS and 7 days of data reduction, analysis, and reporting.

Noteworthy experimental notes recorded in logbook:

1. On July 16, a pulse rejection routine was added to the LabView analysis resulting in the creation of version 3 of the program.
2. In general, laser power stabilizers were not used in conjunction with the pyroelectric detector. Because we have low signals on the 10's of millivolt range and high noise in the 1 millivolt range use of a power stabilizer at 20 % to 50 % throughput caused a significant reduction in signal-to-noise.

Information about data files:

1. Full data files for the scale transfer irradiance calibration of NASA pyro #2 are located on Elwood under:

\\cfs2e.nist.gov\685\internal\G04\Sircus\SIRCUS\Calibrations\SIRCUS Calibrations\FY 2019 Calibrations\Pyros and new IR scale

Data file for the irradiance responsivity scale of NASA pyro #2: "NASA Pyro #2_Irradiance Responsivity from T-01 and Reflectance.xlsx"

2. Full data files for the radiance calibration of GLAMR exIGA are located on Elwood under:

\\cfs2e.nist.gov\685\internal\G04\Sircus\SIRCUS\Calibrations\SIRCUS Calibrations\FY 2019 Calibrations\GLAMR\GLAMR exIGA

Data file for the full spectral absolute radiance responsivity of GLAMR exIGA: "Radiance Responsivity GLAMR exIGA combined data.xlsx"

The files located in these directories are meant for internal NIST use only. Please do not distribute without authorization.

References

1. Brown, S. W., Eppeldauer, G. P. & Lykke, K. R. Facility for spectral irradiance and radiance responsivity calibrations using uniform sources. *Appl. Opt.*, **AO 45**, 8218–8237 (2006).
2. Woodward, J. T. *et al.* Invited Article: Advances in tunable laser-based radiometric calibration applications at the National Institute of Standards and Technology, USA. *Review of Scientific Instruments* **89**, 091301 (2018).
3. Houston, J. M. & Rice, J. P. NIST reference cryogenic radiometer designed for versatile performance. *Metrologia* **43**, S31 (2006).
4. Alberding, B. G. & Woodward, J. T. Report of Test for the Absolute Spectral Irradiance Responsivity of the Silicon Trap Detector T-01 from T-06. (2018).
5. Shaw, P.-S. Report of Calibration for SIRCUS Si Trap Detectors T06 and T04 from 475 nm to 1000 nm. (2016).
6. Shaw, P.-S. Report of Calibration for SIRCUS Trap Detectors T06 and T04 from 364 nm to 470 nm. (2017).
7. Hanssen, L. Report of Calibration: 38075S Special Tests Infrared Reflectance, Transmittance, and Emittance of Materials for a Pyroelectric Detector Witness Sample, Order Item No.: O-00000000469. (2019).
8. Gardner, J. L. Uncertainties in Interpolated Spectral Data. *J. Res. Natl. Inst. Stand. Technol.* **108**, 69–78 (2003).

Distribution Restrictions: None

Tabulated calibration data files were provided along with this report.

Filename: "NASA Pyro #2_Irradiance Responsivity from T-01 and Reflectance.xlsx"
"Radiance Responsivity GLAMR exIGA combined data.xlsx"

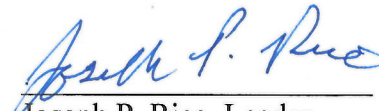
This calibration report shall not be reproduced, except in full, without written approval by NIST.

Prepared by:

Approved by:



Brian G. Alberding
Remote Sensing Group
Sensor Science Division
Physical Measurement Laboratory
(301) 975-4664



Joseph P. Rice, Leader
Remote Sensing Group
Sensor Science Division
Physical Measurement Laboratory
(301) 975-2133